Powder Technology 314 (2017) 281–290

Contents lists available at ScienceDirect

Powder Technology

journal homepage: www.elsevier.com/locate/powtec

Large-eddy simulation of turbulent preferential concentration and collision of bidisperse heavy particles in isotropic turbulence

Jincai Chen, Guodong Jin*

LNM, Institute of Mechanics, Chinese Academy of Sciences, Beijing 100190, China
School of Engineering Science, University of Chinese Academy of Sciences, Beijing 100049, China

ARTICLE INFO

Article history:
Received 30 May 2016
Received in revised form 19 December 2016
Accepted 22 December 2016
Available online 26 December 2016

Keywords:
Particle-laden turbulence
Large-eddy simulation
Subgrid scale motion
Bidisperse particles
Preferential concentration
Collision rate

ABSTRACT

Particle-laden turbulent flows are ubiquitous in natural and engineering flows. The preferential concentration and pair-statistics of heavy particles at small and intermediate Stokes numbers are mainly related to the small-scale motions, which are missing in conventional large-eddy simulation (LES). Therefore, studies on the effects of subgrid scale (SGS) motions on particle-pair statistics are significant. This paper will study the effects of SGS motions on the collision-related statistics of a bidisperse system that involves two groups of particles at different Stokes numbers using a direct numerical simulation (DNS), filtered DNS (FDNS) and LES. Compared with a monodisperse system at a single Stokes number, the relative error of the collision rates in the bidisperse system is much smaller than that in the monodisperse one. For given filter widths and Stokes numbers, the relative errors between the FDNS and LES are much smaller than their relative errors to DNS, implying that the error caused by the filtering operation in LES plays a leading role in the overall error of the particle collision rate at Stokes numbers less than 3. A particle SGS model is, thus, necessary to consider the effect of SGS motions on bidisperse heavy particles.

1. Introduction

Heavy particle-laden turbulent flows are ubiquitous in environmental and engineering flows. Typical examples include the particles in a turbulent fluidized bed and a pneumatic system [1–10], the radioactive particles in nuclear reactors and pipes in a plant [11–14], and warm rain droplets in a cloud [15,16]. The inertia of heavy particles is usually characterized by the Stokes number, St_K, which is the ratio of the particle relaxation time scale τ_p to the turbulent Kolmogorov time scale τ_K. There are two clustering mechanisms of heavy particles at different Stokes numbers caused by the dynamic interaction between the particles and turbulent structures at different space-time scales. When the particle Stokes number is small, the divergence of the particle velocity field (a measure of the compressibility of the particle velocity field or the level of the clustering of particles) is determined by $\nabla\cdot\mathbf{v}_p = -\tau_p(\mathbf{S}^2 - \mathbf{\Omega}^2)$ [17], where $\mathbf{S}$ and $\mathbf{\Omega}$ are the strain rate tensor and the vorticity tensor, respectively. Thus, the heavy particles at small Stokes numbers tend to accumulate in the regions of low vorticity and high strain rate in turbulent flow fields with a negative divergence of the particle velocity field. This mechanism, which is termed preferential concentration, is caused by the centrifugal force of the eddies acting on the particles and can enhance the particle collision kernel up to one or two orders [18–20]. It is observed that the preferential concentration of heavy particles at small Stokes numbers is mainly related to the small-scale motions. Although the small-scale motions possess very little turbulent kinetic energy, they possess a large portion of enstrophy, which indicates that the vorticity is strong at small scales, leading to a large negative divergence of the particle velocity field. However, the "centrifuge mechanism" is no longer appropriate when the particle Stokes numbers are very large ($St_K \gg 1$). Instead, a very different clustering mechanism, named the multiplicative random process, is found to contribute significantly to the clustering of heavy particles. In this regime, small volume elements in the dissipative dynamical systems randomly expand and contract. Depending on whether the random product of expansion and contraction factors increases or decreases at long times, we can observe fractal clustering [21–23]. The two clustering mechanisms compete for particles at intermediate Stokes numbers. In addition, gravity has also been proven to play a critical role in particle-pair statistics[24–29], such as the radial distribution function (RDF) and the radial relative velocity (RRV) of inertial particles. In the monodisperse systems, gravity reduces the RDF of particles when $St_K < 1$ whereas it enhances the RDF of particles when $St_K > 1$. Both the RRV and the collision rate of inertial particles are reduced by gravity over the whole range of

* Corresponding author at: LNM, Institute of Mechanics, Chinese Academy of Sciences, Beijing 100190, China.
E-mail address: gdjin@lnm.imech.ac.cn (G. Jin).

http://dx.doi.org/10.1016/j.powtec.2016.12.069
0032-5910/

St_K [30]. It is noteworthy that the effects of gravity on the particle-pair statistics are small when $St_K < 1$; therefore, simply neglecting the gravity effect for heavy particles at small Stokes numbers in LES might lead to the over-prediction of the particle-pair statistics. We shall leave the effects of gravity on particle-pair statistics of bidisperse particle for a future study and focus on the effects of small-scale turbulent motions on the particle-pair statistics of bidisperse particles in this work. Particles in turbulent flows usually have a broad size spectrum because of coagulation or atomization; thus, they have different relaxation time scales. These polydisperse particles will selectively respond to eddies of different time scales in turbulent flows. A bidisperse system consisting of two groups of particles at Stokes number St_{K1} and St_{K2} was systematically studied using a direct numerical simulation (DNS) [31]. The two groups of particles were found to cluster in different regions of a vortex, resulting in a reduction in the accumulation effect for the bidisperse system. The radial relative velocity is bounded below by the level of clustering in a monodisperse system due to a differential inertia effect. The inertial polydispersity enhances the turbulent transport effect but weakens the accumulation effect relative to a monodisperse system. The turbulent collision kernel determined by the accumulation effect and the turbulent transport effect is one of the essential components in the classical Smoluchowski coagulation equation [32], which governs the population balance of particle number density in a polydisperse system.

In recent years, large-eddy simulation (LES) of turbulent flows has become a potential method and attracted intensive studies [33–37]. In LES, the large scale unsteady turbulent motions can be explicitly resolved, whereas the effects of the smaller scale motions are modeled. Therefore, LES can characterize the non-equilibrium relaxation processes due to the interaction between inertial particles and turbulent coherent structures. Zhou [34] has reviewed the recent developments in the LES method for the two-fluid model in predicting swirling flows. The two-fluid LES method provides better performance in predicting particle statistics than two-fluid RANS modeling. Large eddy simulations have been performed to simulate the triboelectric charging in pneumatic powder transport using the Eulerian-Lagrangian method, where the complex interaction between turbulence and the triboelectric charging is resolved [36]. Four-way coupled Eulerian-Lagrangian LES predictions of particle agglomeration in a vertical turbulent channel flow are conducted, and different influencing parameters on the agglomeration process are systematically studied [35]. In the above studies, the unsteady interaction between particles and the turbulent structures can, thus, be described more accurately than the Reynolds averaged Navier–Stokes (RANS) method (which is widely used in engineering flows). However, the preferential concentration of heavy particles at small and intermediate Stokes numbers is mainly related to the small-scale motions that are missing in LES. Therefore, the study on the effects of the subgrid scale (SGS) motions on the collision-related statistics of heavy particles is of significance.

We have previously studied the effects of SGS motions on the collision-related statistics of a monodisperse system, that is, the effects of the SGS motions on the relative velocity and radial distribution function at contact and the collision rates [20]. Our previous work suggests that a particle SGS model is necessary to represent the effects of SGS fluid motions on monodisperse systems. Different types of particle SGS models have been developed for improving the predictive accuracy of particle statistics using LES [38–41]. The Approximate Deconvolution Method (ADM) [39,42,43] and the differential filter method [44] are used to recover the turbulent energy near and above the resolved scales in LES. Although ADM can partially recover the energy spectrum near the cut-off wavenumber [45,46], it cannot recover the SGS fluid motions below the filter width, which can strongly affect the level of clustering of heavy particles at small Stokes numbers. The Langevin-type models have been constructed for SGS motions experienced by particles [39,47,48]. However, this type of model only works well for predicting single-particle statistics [38]. To predict two-particle and multi-particle statistics, a Lagrangian subgrid model (LSGS) was introduced by Mazzitelli et al. [40]. The LSGS model describes both the turbulent temporal and spatial correlations; thus, it works well for the pair and tetrad dispersions. Recently, Ray and Collins [33,49] used the Kinematic Simulation based SubGrid Model (KSSGM) to predict RDF and RRV of inertial particles. The KSSGM recovers the subgrid spectrum well and accurately predicts the RDF for $St_K \geq 2$ and RRV for the whole range of St_K. Because all these models are developed primarily for the monodisperse systems, a proper particle SGS model for bidisperse systems must be constructed. To check whether the above models can be applied in a bidisperse system, the effects of SGS motions on the statistics of a bidisperse case must be first investigated. The objective of this paper is to extend the method used in [20] to study the effects of SGS motions on the collision-related statistics of a bidisperse system using the DNS, FDNS and LES.

The organization of this paper is as follows: the mathematical equations used for turbulent flows and particle motions are given in Section 2. The flow parameters are also presented in Section 2. We discuss the effects of filtered width on the collision rate in Section 3. Next, we discuss the effects of filtering operation and the subgrid scale model error on the collision rate in Section 4. We present the conclusions drawn in Section 5.

2. Mathematical equations and flow parameters

2.1. Navier–Stokes equations for DNS

In spectral space, the Navier–Stokes equation for the isotropic and incompressible turbulence in a box of $(2\pi)^3$ can be represented as

$$\left(\frac{\partial}{\partial t}+\nu k^2\right)\hat{\boldsymbol{u}}(\boldsymbol{k},t)=\boldsymbol{P}(\boldsymbol{k})\mathcal{F}(\boldsymbol{u}\times\boldsymbol{\omega})+\hat{\boldsymbol{f}}(\boldsymbol{k},t), \tag{1}$$

where $\hat{\boldsymbol{u}}(\boldsymbol{k},t)$ is a Fourier coefficient of fluid velocity $\boldsymbol{u}$, $\boldsymbol{k}=(k_x,k_y,k_z)$ the wavenumber vector with $k=|\boldsymbol{k}|$, ν fluid kinematical viscosity. $\boldsymbol{\omega}=\nabla\times\boldsymbol{u}$ is the vorticity in physical space. The projection tensor $\boldsymbol{P}_{ij}=\delta_{ij}-k_jk_m/k^2(j,m=1,2,3)$, and $\mathcal{F}$ denotes a Fourier transform. The random artificial force $\hat{\boldsymbol{f}}(\boldsymbol{k},t)$ proposed by Eswaran and Pope [50] is used to drive and maintain the turbulent flow.

2.2. Filtered DNS

The filtered velocity field is calculated from the Fourier coefficients obtained from DNS using a sharp spectral filter:

$$\tilde{\boldsymbol{u}}(\boldsymbol{x},t)=\mathcal{F}^{-1}\begin{cases}\hat{\boldsymbol{u}}(\boldsymbol{k},t) & \text{if}\quad |k|\in[1,k_{cf}],\\ 0 & \text{if}\quad |k|\in(k_{cf},k_{\max}],\end{cases} \tag{2}$$

where $\tilde{\boldsymbol{u}}(\boldsymbol{x},t)$ is the filtered velocity in physical space, k_{cf} the cutoff wavenumber and $k_{\max}$ the maximum wavenumber used in DNS. By varying the cutoff wavenumber k_{cf}, we can study the effects of filter width on the particle collision-related statistics.

2.3. Large-eddy simulation (LES)

The LES of isotropic turbulence is performed on coarser grids using the same pseudo-spectral method and large-scale forcing scheme as DNS. The governing equation in LES is given by

$$\left\{\frac{\partial}{\partial t}+[\nu+\nu_e(k|k_c)]k^2\right\}\hat{\tilde{\boldsymbol{u}}}(\boldsymbol{\omega},t)=\boldsymbol{P}(\boldsymbol{k})\mathcal{F}(\tilde{\boldsymbol{u}}\times\tilde{\boldsymbol{\omega}})+\hat{\boldsymbol{f}}(\boldsymbol{k},t), \tag{3}$$

where $\bar{\boldsymbol{u}}$ and $\bar{\boldsymbol{\omega}}$ are the resolved velocity and vorticity in physical space, $\hat{\bar{\boldsymbol{u}}}(\boldsymbol{k},t)$ is the resolved velocity in spectral space, $\nu_e(k|k_c)$ the spectral eddy viscosity which can be expressed as [51,52]

$$\nu_e(k|k_c) = \nu_e^+(k/k_c)\sqrt{\frac{E(k_c)}{k_c}}, \tag{4}$$

and

$$\nu_e^+(k/k_c) = C_K^{-3/2}[0.441 + 15.2\exp\ (-3.03k_c/k)], \tag{5}$$

where $C_K = 2.1$, k_c is the cutoff wavenumber used in LES and $E(k)$ is the energy spectrum of turbulent energy. If we neglect the numerical error by virtue of the spectral method, there are filtering error and SGS modeling error in real LES. Filtering error comes from the missing of SGS velocity due to the filtering operation [53]. The modeling error comes from the fact that the LES only gives an approximation and cannot provide the same filtered velocity as FDNS due to the limitations of currently available SGS models [54–56].

2.4. Equations for particle motion

The discrete phase is composed of 400,000 solid, spherical particles with diameter $d_p = 0.5\eta$. Since the particle density ρ_p is much larger than the fluid density ρ_f, $\rho_p \gg \rho_f$, the forces on a small particle can be simplified as drag force. Then, the governing equations for a single particle can be written as [57]

$$\frac{\mathrm{d}\boldsymbol{x}_p(t)}{\mathrm{d}t} = \boldsymbol{v}_p(t), \tag{6}$$

$$\frac{\mathrm{d}\boldsymbol{v}_p(t)}{\mathrm{d}t} = \frac{(\boldsymbol{u}(\boldsymbol{x}_p(t),t) - \boldsymbol{v}_p(t))f}{\tau_p}, \tag{7}$$

where $\boldsymbol{x}_p(t)$ and $\boldsymbol{v}_p(t)$ are particle position and velocity at time t. $\boldsymbol{u}(\boldsymbol{x}_p(t),t)$ is the fluid velocity seen by a particle. The velocity is obtained from flow field by a three-dimensional six-point Lagrangian interpolation scheme [58]. f is the nonlinear drag correction coefficient:

$$f(Re_p) = 1 + 0.15Re_p^{0.687}, \tag{8}$$

which is determined by the instantaneous value of the particle Reynolds number:

$$Re_p = \frac{|\boldsymbol{u} - \boldsymbol{v}_p|d_p}{\nu}. \tag{9}$$

2.5. Parameters of the turbulent flow field

Table 1 lists the flow parameters of the isotropic turbulent flow simulated in the present study. The root mean square (rms) of turbulent fluctuation velocity, u', is computed from the turbulent energy spectrum $E(k)$,

$$u' = \sqrt{\frac{1}{3}\langle \boldsymbol{u}\cdot\boldsymbol{u}\rangle} = \sqrt{\frac{2}{3}\int_{k_0}^{k_{\max}} E(k)\mathrm{d}k}, \tag{10}$$

and the average dissipation rate ϵ is defined as,

$$\epsilon = \int_{k_0}^{k_{\max}} 2\nu k^2 E(k)\mathrm{d}k. \tag{11}$$

Table 1
Flow parameters of the isotropic turbulent flow.

Parameters	DNS (256^3)	LES (64^3)
Reynolds number Re_λ	102.92	–
rms velocity u'	19.42	18.52
Dissipation rate ϵ	3771.4	3434.8
Kolmogorov length scale η	0.0134	–
Kolmogorov time scale τ_K	0.0037	–
Kolmogorov velocity scale v_K	3.628	–
Spatial resolution $k_{\max}\eta$	1.124	–
Integral length scale L_f	0.9946	–
Large eddy turnover time scale T_E	0.1056	–
Viscosity ν	0.0488	0.0488

The turbulent Kolmogorov scales are

$$\eta = (\nu^3/\epsilon)^{0.25}, \quad \tau_K = (\nu/\epsilon)^{0.5}, \quad v_K = (\epsilon\nu)^{0.25}. \tag{12}$$

Taylor-microscale Reynolds number $R_\lambda = u'\lambda/\nu$, where λ is the transverse Taylor microscale $\lambda = (15\nu u'^2/\epsilon)^{0.5}$, large-eddy turnover time scale $T_E = u'^2/\epsilon$, and the integral length scale

$$L_f = \left(\frac{3\pi}{4}\int_{k_0}^{k_{\max}} k^{-1}E(k)\mathrm{d}k\right) \Big/ \int_{k_0}^{k_{\max}} E(k)\mathrm{d}k. \tag{13}$$

In LES, the dissipation rate is calculated as,

$$\epsilon = \int_{k_0}^{k_c} 2[\nu + \nu_e(k|k_c)]k^2E(k)\mathrm{d}k. \tag{14}$$

Fig. 1 plots the energy spectrum from the DNS of isotropic turbulence at a resolution of 256^3. Here, the vertical dashed lines shown in Fig. 1 represent the different cutoff wavenumbers in the FDNS. As shown in Fig. 1, the energy spectrum does not decrease to zero but increases and goes up a bit near the cutoff wavenumber $k_{\max}$ in the DNS result. This is a truncation error when we use finite wavenumbers in spectral space to express the nonlinear advection term in the Navier–Stokes equations. If the cutoff wavenumber $k_{\max}$ cannot fully resolve the minimum length scale in the turbulent flow, or $\eta k_{\max} \sim 1$, then the turbulent energy will transfer to a smaller scale through the cascade process and accumulate near the cutoff wavenumber.

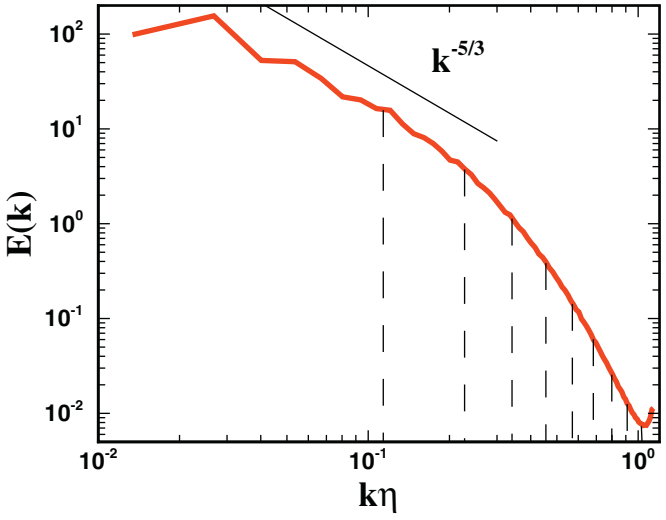

Fig. 1. The energy spectrum of the simulated flow in DNS (256^3). The vertical dashed lines denote different cutoff locations in FDNS.

For $E(k)$ to drop to zero, we must increase η, that is, we can increase the value of $k_{\max}\eta$ to a large value ($\eta k_{\max} \gg 1$) at the cost of a simulated flow at a lower Reynolds number, such that the energy spectrum will decrease to nearly zero, and all the turbulent energy will be dissipated by molecular viscosity.

3. Effects of filter width on collision-related quantities of the bidisperse system

For a monodisperse system with N_p particles, the turbulent collision rate in a turbulent flow can be expressed as [18,19]

$$\langle N_c \rangle = 2\pi \langle |Wr(R)| \rangle \langle g(R) \rangle \frac{n_0^2}{2}, \tag{15}$$

where $\langle |Wr(R)| \rangle$ is the mean radial relative velocity at contact, R is the collision radius, $\langle g(R) \rangle$ is the mean radial distribution function at contact, n_0 is the average number density, and $n_0 = N_p/(2\pi)^3$. For a bidisperse system with two groups of particles, the particle numbers are N_{p1} and N_{p2}, and the collision rate between the two groups of particles $\langle N_{c12} \rangle$ is [31]

$$\langle N_{c12} \rangle = 2\pi \langle |Wr_{12}(R)| \rangle \langle g_{12}(R) \rangle n_1 n_2, \tag{16}$$

where $\langle |Wr_{12}(R)| \rangle$ is the mean radial relative velocity at contact between the two groups of particles, $\langle g_{12}(R) \rangle$ is the mean radial distribution function between the two groups of particles at contact, and $n_1 = N_{p1}/(2\pi)^3$ and $n_2 = N_{p2}/(2\pi)^3$.

To study the effects of filter width on the collision-related quantities, we compute the RDF, RRV and collision rates of particles at different values of the Stokes number $St_{K2} = 0.2, 0.5$ and 1.5 while we keep $St_{K1} = 1$ in the FDNS flow fields at different cutoff wavenumbers $k_{cf} = 64, 42$ and 21 (or $k_{cf}/k_{\max} = 0.75, 0.5$ and 0.25) with $k_{\max} = 84$ in the DNS. We have discussed the effects of filter width on the collision-related quantities for the monodisperse particles in Ref. [20]; however, the effects of filter width on these statistics for bidisperse particles are still unknown. Therefore, we would seek to compare the effects of filter width on the two different systems in this study. Figs. 2–4 show the variations of the relative errors of the RDF, the RRV, and the collision rate to the results of the DNS with dimensionless filter width, respectively. We can observe that,

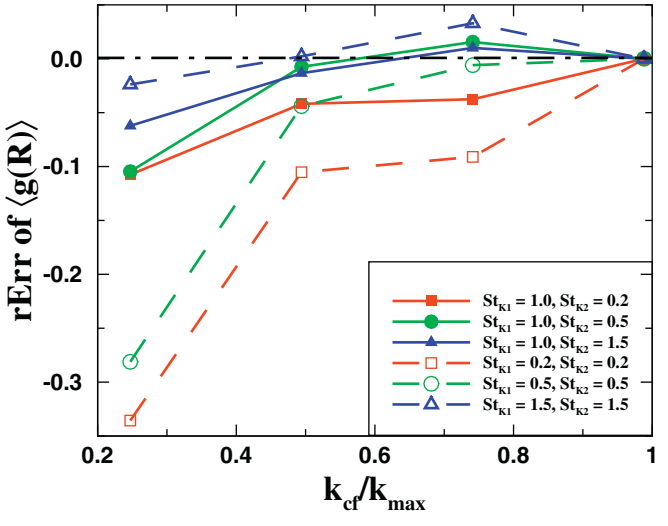

Fig. 2. Effects of filter width on the relative error $rErr = (\alpha_{FDNS} - \alpha_{DNS})/\alpha_{DNS}$ of RDFs for monodisperse and bidisperse of particles at different Stokes number. Solid lines denote bidisperse system, dashed lines denote monodisperse system. Square symbol: $St_{K2} = 0.2$; circle symbol: $St_{K2} = 0.5$; delta symbol: $St_{K2} = 1.5$.

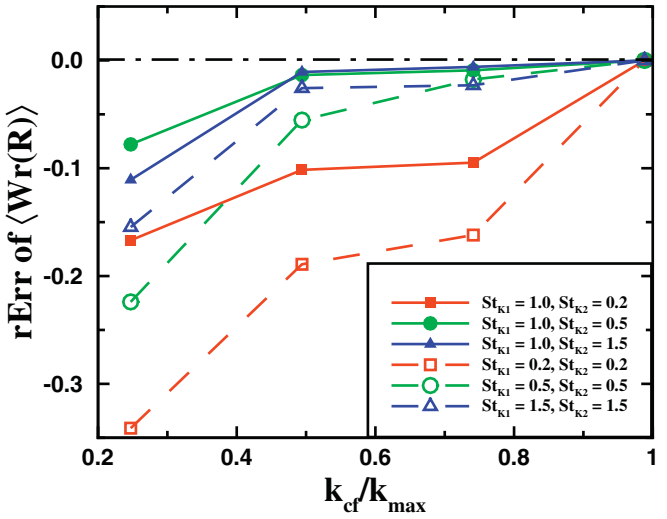

Fig. 3. Effects of filter width on the relative error $rErr = (\alpha_{FDNS} - \alpha_{DNS})/\alpha_{DNS}$ of RRVs for monodisperse and bidisperse of particles at different Stokes number. The legends are the same as Fig. 2.

for particles at a given Stokes number, the relative error increases with filter width and the relative errors are not the same for the RDF, the RRV and the collision rate. In the bidisperse system, when $k_{cf} = 21$ ($k_{cf}/k_{\max} = 0.25$) and $St_{K2} = 0.5$, the relative errors for the RDF, the RRV, and the collision rate are −0.10459, −0.07789, and −0.18863, respectively. For a given filter width, the filtering operation has different effects for particles at different Stokes number because particles with different Stokes numbers respond to eddies at different scales. Compared to the monodisperse system, the relative errors of the RDF, the RRV and the collision rate are different. We can observe that for $k_{cf} = 21$ ($k_{cf}/k_{\max} = 0.25$) and $St_{K2} < 1$, the relative errors are less than the errors in the monodisperse system, whereas for $St_{K2} > 1$, the relative error of the RDF is greater than that in the monodisperse system.

4. Effects of SGS model error on collision-related quantities of the bidisperse system

The spectral eddy viscosity model used to close the Navier–Stokes equation is over-dissipative, making the vortical structures in the LES

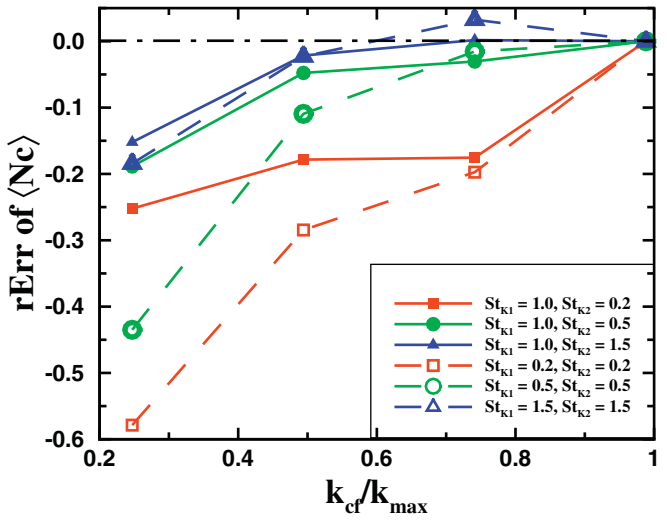

Fig. 4. Effects of filter width on the relative error $rErr = (\alpha_{FDNS} - \alpha_{DNS})/\alpha_{DNS}$ of mean collision rate for monodisperse and bidisperse of particles at different Stokes number. The legends are the same as Fig. 2.

flow field smoother than that in the ideal LES, that is, the FDNS. In this section, we study the effects of the spectral eddy viscosity and the SGS turbulent motions on the RDF and the RRV by comparing the results from the DNS, the FDNS and the LES, where the cutoff wavenumber k_{cf} in the LES and the FDNS are the same. For a given cutoff wavenumber k_{cf}, the differences between the results from the DNS and the FDNS denote the contributions of the SGS motions and the differences between the FDNS and the LES denote the contributions of the SGS model error because the FDNS can be regarded as an ideal LES.

4.1. Radial distribution function

In this subsection, we set $k_{cf} = 21$, the spatial resolution in the 256^3 DNS is four times of those in the FDNS and the LES, that is, $\Delta x_{LES} = \Delta x_{FDNS} = 4\Delta x_{DNS}$.

Fig. 5 shows the variation of the RDF at contact with particle Stokes number St_{K2}, where $St_{K1} = 1$. The solid lines denote the results of the bidisperse system, whereas the dashed lines denote the results of the monodisperse system. To validate our DNS results, we also plot the DNS results from Ref. [30] for comparison, where the particle radii range from 0.017η to 0.101η. These particle radii are smaller than the particle radius, $a_p = 0.25\eta$, used in this study. Because $g(r)$ decreases with increasing r, it is reasonable that the RDFs in Ref. [30] are larger than our DNS results. However, our results are in good qualitative agreement with those from Ref. [30] with the same tendency that $g(r)$ reaches a maximum value at $St_K \sim 1$ and $g(r) \to 1$ at very small and very large Stokes numbers. From Fig. 5, the RDFs in the monodisperse system are found to be larger than those in the bidisperse system for DNS, FDNS and LES. For finite inertial particles, the RDF in the monodisperse particles is the upper limit of that in the bidisperse system. In the bidisperse system, the two groups of particles with different relaxation times respond to the eddies at different scales; therefore, the two groups of particles accumulate in different regions in the turbulent flow field. The level of clustering of the two groups of particles is, thus, reduced. The correlation coefficient of the concentration fields can be defined as [31]

$$\rho_{12} = \frac{\langle (c_1 - \bar{c}_1)(c_2 - \bar{c}_2)\rangle}{\left[\langle (c_1 - \bar{c}_1)^2\rangle \langle (c_2 - \bar{c}_2)^2\rangle\right]^{1/2}}, \tag{17}$$

where $\bar{c}_i = N_{p,i}/V$ is the mean number density of group $i (i = 1, 2)$, V is the volume of the flow domain, c_1 and c_2 are the local number density. For the bidisperse system, the RDF $\langle g_{12}(R)\rangle$ can be expressed as [31]

$$\langle g_{12}(R)\rangle = 1 + \rho_{12}[(\langle g_{11}(R)\rangle - 1)(\langle g_{22}(R)\rangle - 1)]^{1/2}, \tag{18}$$

where $\langle g_{11}(R)\rangle$ and $\langle g_{22}(R)\rangle$ are the RDFs of the monodisperse system for groups 1 and 2, respectively. We find $\langle g_{22}(R)\rangle_{DNS} > \langle g_{22}(R)\rangle_{FDNS} > \langle g_{22}(R)\rangle_{LES}$ for $St_K < 1$. This is expected because small-scale motions are responsible for the clustering of particles at small Stokes numbers. The filtering operation reduces the level of clustering of particles at $St_K < 1$, whereas for $St_K > 1$, $\langle g_{22}(R)\rangle_{DNS} < \langle g_{22}(R)\rangle_{FDNS} < \langle g_{22}(R)\rangle_{LES}$, implying that the resolved motions are responsible for the clustering of particles at large Stokes numbers, and the random SGS motions tend to make particles homogeneous.

The results for the bidisperse system show that for $St_{K2} > 1$, $\langle g_{12}(R)\rangle_{DNS} > \langle g_{12}(R)\rangle_{FDNS} > \langle g_{12}(R)\rangle_{LES}$. In our simulated system, the Stokes number for the first group is $St_{K1} = 1$. When $St_{K2} > 1$, the large scale resolved scale motions are responsible for the clustering of particles and $\langle g_{22}(R)\rangle_{LES} > \langle g_{22}(R)\rangle_{FDNS} > \langle g_{22}(R)\rangle_{DNS}$. In contrast, the small-scale motions are still responsible for the clustering of the first group of particles, $\langle g_{11}(R)\rangle_{LES} < \langle g_{11}(R)\rangle_{FDNS} < \langle g_{11}(R)\rangle_{DNS}$. Thus, the under-prediction of $\langle g_{11}(R)\rangle$ in the LES and the FDNS cancels out the over-prediction of $\langle g_{22}(R)\rangle$ in the LES and the FDNS.

Fig. 6 shows the relative error of the RDF in the FDNS and the LES for the monodisperse and bidisperse particles. The relative errors are found to reach maximum values at $St_K = 0.5$ for the monodisperse particles. The relative errors decrease with increasing Stokes numbers, implying that the contribution of the SGS motions play diminishing roles in the clustering of particles with the increase of particles Stokes numbers.

From Fig. 6, we also find that for bidisperse system and fixed Stokes number $St_{K1} = 1$, the relative error to DNS is much smaller than that for the monodisperse system overall. When $St_{K2} < 1$, the maximum relative error in the bidisperse system is half of that in the monodisperse system. When $St_{K2} > 2$, the FDNS and the LES slightly under-predict the RDFs with relative errors of less than 5% for the bidisperse system but over-predict the RDFs with larger relative errors of approximately 10% for the monodisperse case.

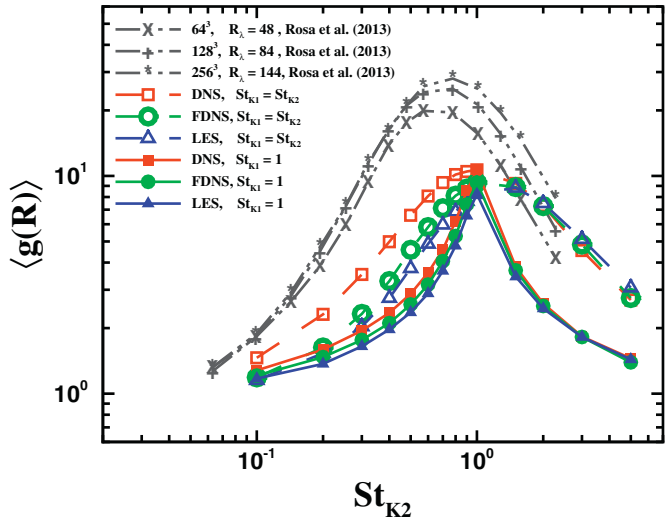

Fig. 5. Variation of RDF with St_{K2} while St_{K1} is fixed to be 1.0 for bidisperse systems and St_{K1} is equal to St_{K2} for monodisperse systems.

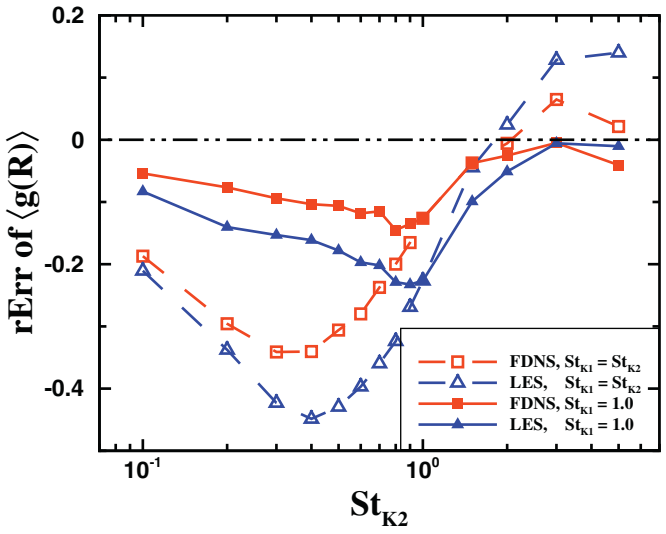

Fig. 6. Variation of the relative error of RDF with St_{K2} while St_{K1} is fixed to be 1.0 for bidisperse systems and St_{K1} is equal to St_{K2} for monodisperse systems.

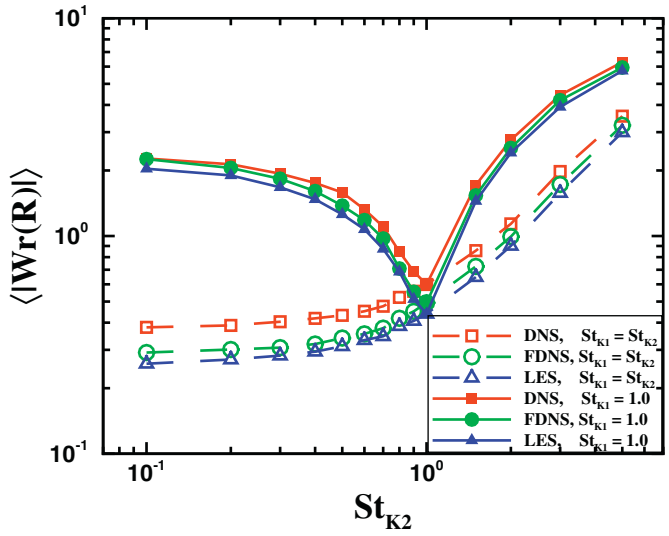

Fig. 7. Variation of RRV with St_{K2} while St_{K1} is fixed to be 1.0 for bidisperse systems and St_{K1} is equal to St_{K2} for monodisperse systems.

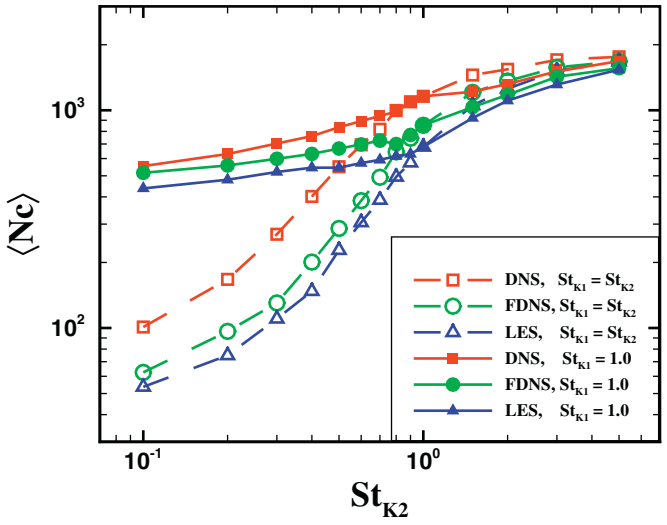

Fig. 9. Variation of the collision rate with St_{K2} while St_{K1} is fixed to be 1.0 for bidisperse systems and St_{K1} is equal to St_{K2} for monodisperse systems.

4.2. Radial relative velocity

Jin et al. [20] have shown that, although the turbulent fluctuating velocity filtered out in the LES and the FDNS are negligible, the turbulent structure and the spatial-temporal correlation of the turbulent flow field become strong, leading to a large relative error of the radial relative velocity at contact for particles at small Stokes numbers. For the bidisperse system, the radial relative velocity increases with the increase of the inertia difference between the two groups of particles, and the relative velocity of the monodisperse system is the lower limit of the bidisperse system. Fig. 7 shows the variation of the relative velocity of the monodisperse system and bidisperse system with Stokes number St_{K2}. The relative velocity of the bidisperse system in the DNS, the FDNS and the LES are all found to be above those of the monodisperse system. There is a point of intersection at $St_{K2} = 1$. As St_{K2} departs from $St_{K2} = 1$, the difference between the bidisperse system and monodisperse system becomes larger.

Fig. 8 shows the variations of relative errors of RRV with particle Stokes number St_{K2}. The dashed lines denote the results of monodisperse particles with $St_{K1} = St_{K2}$, whereas the solid lines denote the results of the bidisperse case with $St_{K1} = 1.0$. The relative errors in the monodisperse system are found to decrease with increasing Stokes number. This may be explained by the fact that the effects of SGS motions on the RRV decrease with increasing Stokes numbers [20]. Next, we consider the new findings of the relative errors in the bidisperse system. From Fig. 8, the relative errors are observed to reach the maximum values of approximately 25% at $St_{K2} = 1.0$ in both the FDNS and the LES. When St_{K2} departs from 1.0, the relative errors gradually decrease to the level of under 10% for the simulated Stokes numbers. Further discussion on the phenomenon will be presented in Section 4.4.

4.3. Collision rate

The collision rate is the combination of particle clustering, measured by $\langle g(R)\rangle$, and the transport effect, measured by the mean RRV. For the monodisperse system, the collision rate increases rapidly

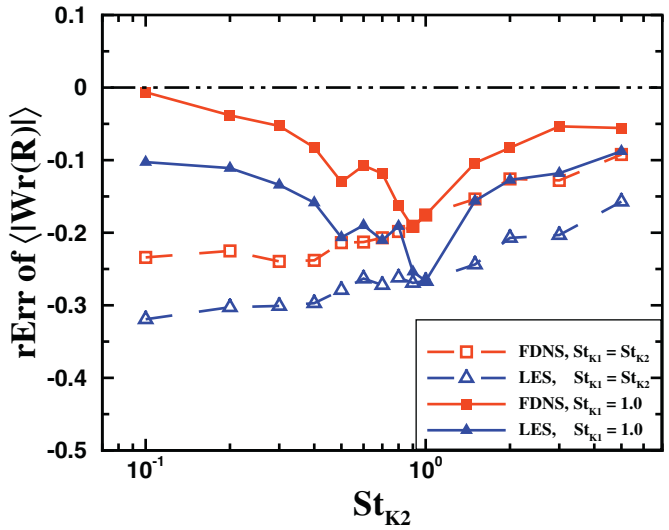

Fig. 8. Variation of the relative error of RRV with St_{K2} while St_{K1} is fixed to be 1.0 for bidisperse systems and St_{K1} is equal to St_{K2} for monodisperse systems.

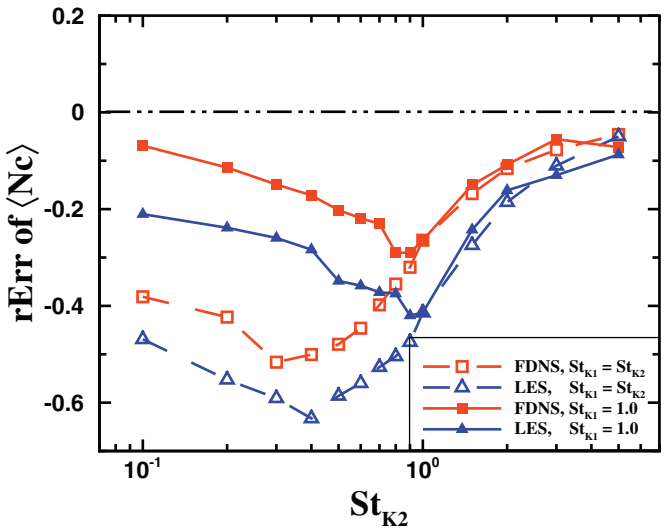

Fig. 10. Variation of relative error of the collision rate with St_{K2} while St_{K1} is fixed to be 1.0 for bidisperse systems and St_{K1} is equal to St_{K2} for monodisperse systems.

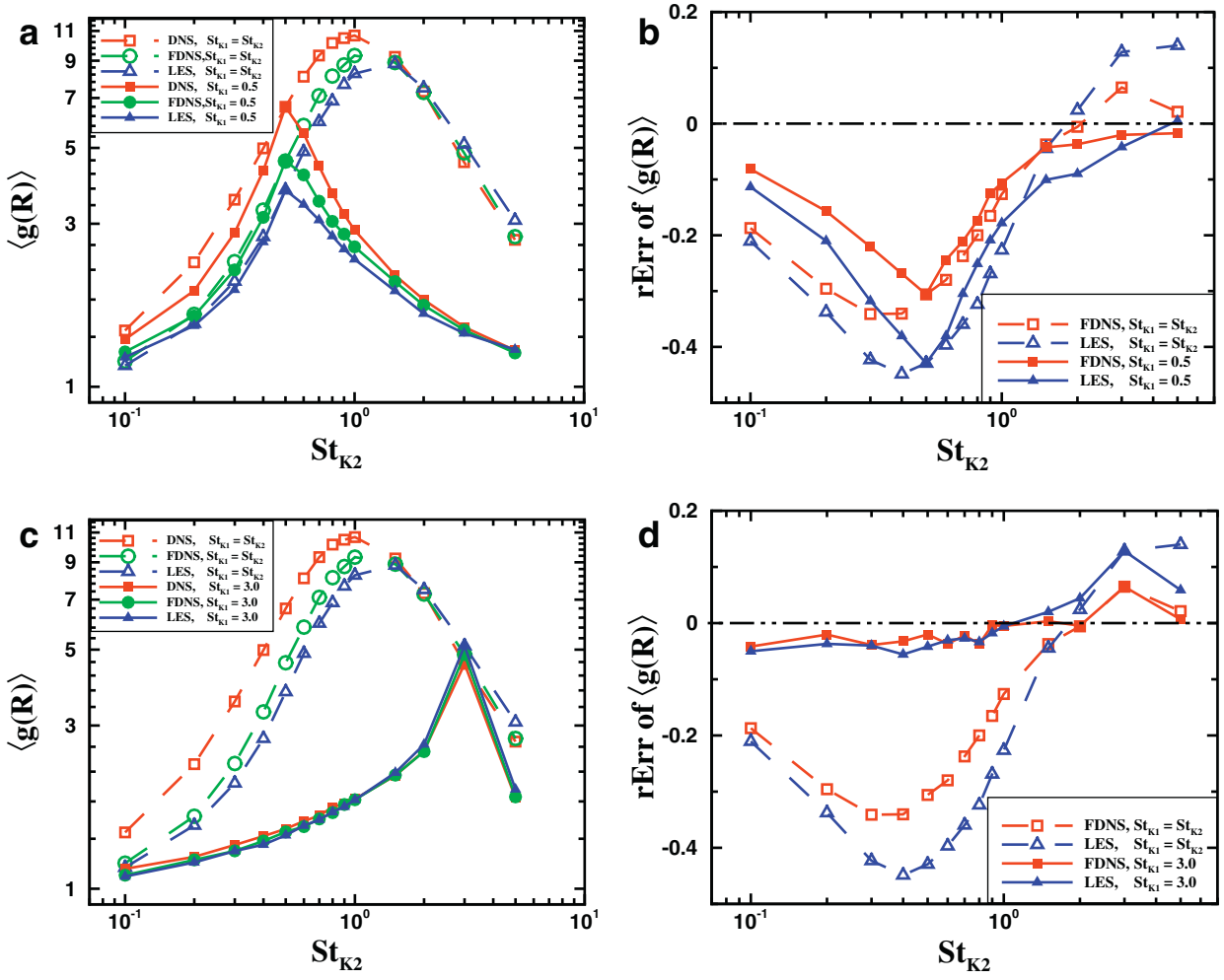

Fig. 11. Variation of RDFs and their relative errors with St_{K2} while St_{K1} is fixed to a constant for bidisperse systems and St_{K1} is equal to St_{K2} for monodisperse systems. (a)–(b): $St_{K1} = 0.5$; (c)–(d): $St_{K1} = 3.0$.

for small Stokes numbers. Because of the canceling of the over-prediction of $\langle g(R)\rangle$ and the under-prediction of $\langle|Wr(R)|\rangle$, the LES and the FDNS can predict the collision rate well for $St_K > 3$.

Fig. 9 shows the variation of collision rate in the monodisperse and bidisperse systems with Stokes number St_{K2}. Compared with the monodisperse system, the curves for the bidisperse system saturate more slowly. For $St_{K2} < 1$, the collision rate for the binary system is higher than that for the monodisperse system, whereas for $St_{K2} > 1$, the collision rate for the binary system is smaller than that for the monodisperse system. From Figs. 7 and 8, the relative velocity for the bidisperse system is found to be much higher than that for the monodisperse system, making the collision rate higher for $St_{K2} < 1$. In contrast, for $St_{K2} > 1$, the radial distribution function for the bidisperse system is smaller than that of the monodisperse system, resulting in a lower collision rate. Because the relative errors for the RDF and the RRV in the bidisperse system are much smaller than those in the monodisperse system, the relative error in the collision rate is much smaller than that in the monodisperse system.

Fig. 10 shows the variations of the relative errors of the collision rate to the DNS with particle Stokes number St_{K2}. Fig. 10 reveals that the relative errors in the binary system are much smaller than those in the monodisperse system. The maximum error reduces from 45% to 30%, and the Stokes number shifts to $St_{K2} = 1$, where the relative error reaches its maximum. Because $St_{K1} = 1$, the bidisperse system becomes a monodisperse system when St_{K2} approaches 1.0. The relative error is smaller in the binary system, and when $St_{K2} > 3$, the LES and the FDNS can give reasonable results. In the bidisperse system, the difference between the DNS and the LES or the FDNS is much larger than that between the FDNS and the LES, implying that the dominating factor of the error in the collision rate is the filtering operation.

4.4. General combination of a bidisperse system with varied St_{K1} and St_{K2}

In the previous sections, we have considered the bidisperse system with St_{K1} fixed to be 1.0. To further understand the effects of filtering and SGS eddy viscosity model on the collision-related quantities of a bidisperse system, we consider two cases, in which $St_{K1} = 0.5$ and $St_{K1} = 3.0$, and St_{K2} varies to produce a more general combination of the bidisperse systems.

We first discuss the variations of the RDFs and their relative errors with St_{K2} under different St_{K1}, as shown in Fig. 11, where (a)–(b) correspond to the case with $St_{K1} = 0.5$ and (c)–(d) correspond to the case with $St_{K1} = 3.0$. Panels (a) and (c) in Fig. 11 show that the RDFs in both bidisperse systems still obey the observation that the RDFs in the monodisperse system are the upper limit of those in the bidisperse system, and the RDFs reach the maximum values at $St_{K2} = St_{K1}$ [31]. A quantitative comparison of the relative errors due to filtering and the SGS eddy viscosity model in the FDNS or the LES is

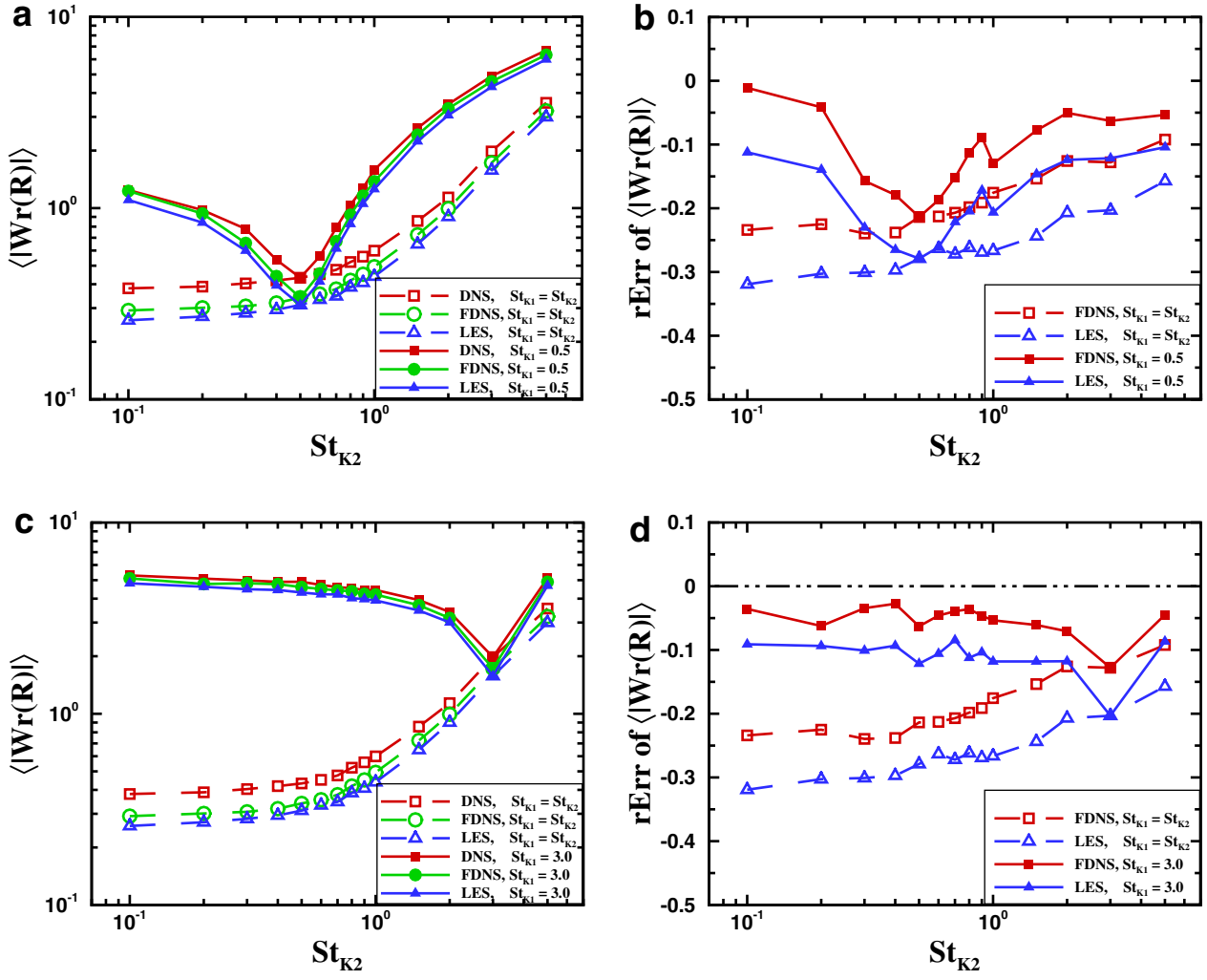

Fig. 12. Variation of RRVs and their relative errors with St_{K2} while St_{K1} is fixed to a constant for bidisperse systems and St_{K1} is equal to St_{K2} for monodisperse systems. (a)–(b): $St_{K1} = 0.5$; (c)–(d): $St_{K1} = 3.0$.

shown in Fig. 11 (b) and (d). The new finding is that the relative errors achieve maximum values at $St_{K2} = St_{K1}$, and they decrease with increasing particle inertia differences. The reason for this result is that particles at different Stokes numbers cluster in different zones of the turbulent field. The influence of filtering on the RDF of bidisperse particles, thus, decreases with increasing inertia differences. It is interesting that FDNS or LES under-predicts the RDF in the bidisperse system with $St_{K1} = 0.5$ but over-predicts the RDF in the bidisperse system with $St_{K1} = 3.0$. The reason for this observation is that the bidisperse system with $St_{K1} = 3.0$ is reduced to the monodisperse case at $St_{K2} = 3.0$, and, thus, the filtering of SGS motions enhances the particle clustering. We can draw a conclusion that there are two important factors affecting the accuracy of the FDNS or the LES in predicting the RDF in the bidisperse system. The first factor is the relative error in the monodisperse case at $St_{K2} = St_{K1}$, which is the upper limit of the error in the bidisperse case. The second factor is the inertia difference between St_{K1} and St_{K2}, which reduces the influence of filtering.

Fig. 12 shows the variations of the RRVs and the relative errors in the FDNS and the LES results to the DNS results for different St_{K1}. From Fig. 12 (a) and (c), the bidisperse systems with $St_{K1} = 0.5$ or $St_{K1} = 3.0$ are found to still obey the observation that the RRV of monodisperse particles is the lower limit of that of bidisperse particles and the later reaches the minimum value at $St_{K2} = St_{K1}$ [31]. By comparing the relative errors of the FDNS or the LES to the DNS, as shown in Fig. 12 (b) and (d), the relative errors in the monodisperse systems are found to be the upper limit of those in the bidisperse systems, where $St_{K1} = 0.5$ or $St_{K1} = 3.0$. The relative errors shift to the maximum values at $St_{K2} = St_{K1}$ and then decrease with increasing inertia differences. For RRV, the larger particle inertia difference leads to the smaller correlation between the two particles, and, thus, filtering and the SGS eddy viscosity model contribute less to the particle velocity correlation.

Finally, we consider the variations of the collision rates and their relative errors, as shown in Fig. 13. Because the collision rate is the combination of the RRV and the RDF, it is expected that the relative error of collision rate in the FDNS or the LES is determined by the particle inertia differences and the relative error at $St_{K2} = St_{K1}$ in the monodisperse system, which is shown in Fig. 13 (b) and (d). When $St_{K1} = 0.5$, the maximum relative error reaches 50%–60% at $St_{K2} = 0.5$, and the relative error gradually decreases with St_{K2} departing from 0.5; when $St_{K1} = 3.0$, the relative errors of collision rates remain small during the whole inertial range because of the small relative error at $St_K = 3.0$ in the monodisperse system.

5. Conclusions

Particle-laden turbulent flows are ubiquitous in natural and engineering flows. The preferential concentration and pair statistics of

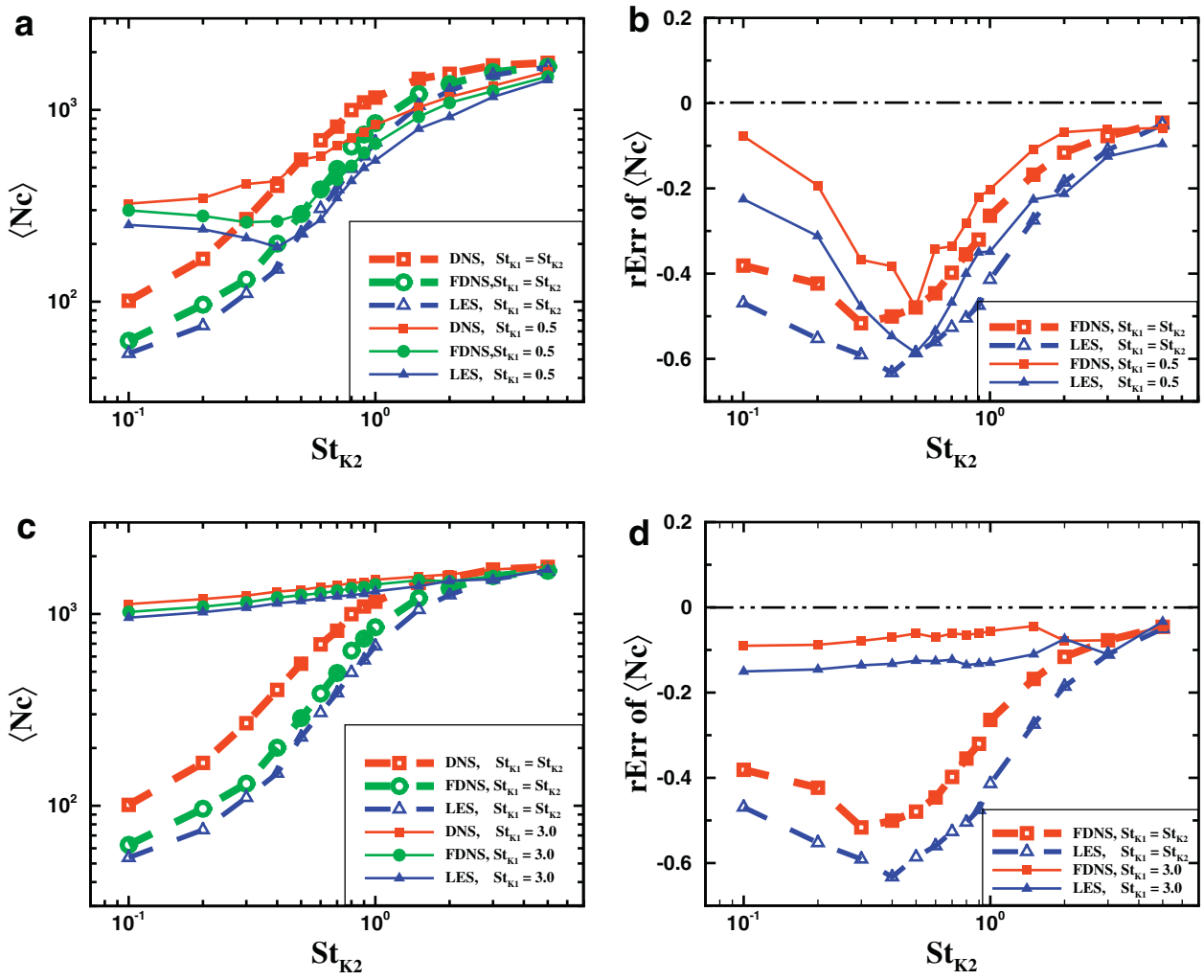

Fig. 13. Variation of collision rates and their relative errors with St_{K2} while St_{K1} is fixed to a constant for bidisperse systems and St_{K1} is equal to St_{K2} for monodisperse systems. (a)–(b): $St_{K1} = 0.5$; (c)–(d): $St_{K1} = 3.0$.

heavy particles at small and intermediate Stokes numbers are mainly related to the small-scale motions, which are missing in large-eddy simulation (LES). Therefore, we focused on the effects of the subgrid scale (SGS) motions on the particle-pair statistics of a bidisperse system involving two groups of particles using direct numerical simulation (DNS), filtered DNS (FDNS) and LES. Compared with the monodisperse system, the relative error of the collision rate in the bidisperse system was found to be much smaller than the monodisperse one. This result can be explained by two important factors. The first factor is the relative error in the monodisperse case at $St_{K2} = St_{k1}$, which is the upper limit of the error in the bidisperse case. The second factor is the inertia difference between St_{K1} and St_{K2}, which reduces the influence of filtering. For given filter widths and Stokes numbers, the relative error between FDNS and LES is much smaller than their relative errors to DNS, implying that the error caused by the filtering operation in LES plays a leading role in the overall error of particle collision rate at Stokes numbers less than 3. Thus, a particle SGS model is necessary to recover the effects of SGS fluid motions on bidisperse particles with different relaxation time scales in future studies. In future work, particle SGS models may be constructed based on the space-time correlation models [59–61]. In these models, the small-scale motions with proper spatial and temporal correlations will be taken into accounted to predict the collision rate of bidisperse particles in turbulent flows [37].

Acknowledgments

This work was supported by the National Natural Science Foundation of China (11472277 and 11232011), Strategic Priority Research Program, CAS (XDB22040104), Key Research Program of Frontier Sciences, CAS (QYZDJ-SSW-SYS002), Science Challenge Program (JCKY2016212A501) and the 973 Program of China (2013CB834100). JGD would like to thank Professor Lian-Ping Wang at University of Delaware, USA for the discussion and help during the work of this paper. The anonymous reviewers are much appreciated for the constructive suggestions to improve the manuscript.

References

[1] X.H. Liu, S.Q. Gao, J.H. Li, Characterizing particle clustering behavior by PDPA measurement for dilute gas-solid flow, Chem. Eng. J. 108 (3) (2005) 193–202.
[2] S.B. Kuang, A.B. Yu, Z.S. Zou, Computational study of flow regimes in vertical pneumatic conveying, Ind. Eng. Chem. Res. 48 (14) (2009) 6846–6858.
[3] B. Wang, K.W. Chu, A.B. Yu, Numerical study of particle-fluid flow in a hydrocyclone, Ind. Eng. Chem. Res. 46 (13) (2007) 4695–4705.
[4] A.W. Vreman, Turbulence attenuation in particle-laden flow in smooth and rough channels, J. Fluid Mech. 773 (2015) 103–136.
[5] S. Benzarti, H. Mhiri, H. Bournot, R. Occelli, Numerical simulation of turbulent fluidized bed with Geldart B particles, Adv. Powder Technol. 25 (6) (2014) 1737–1747.

[6] T.J. O'Brien, A multiphase turbulence theory for gas-solid flows: I. Continuity and momentum equations with Favre-averaging, Powder Technol. 265 (2014) 83–87.
[7] J. Capecelatro, O. Desjardins, R.O. Fox, Numerical study of collisional particle dynamics in cluster-induced turbulence, J. Fluid Mech. 747 (2014) R2:1–13.
[8] M. Dehghan, H.B. Tabrizi, Turbulence effects on the granular model of particle motion in a boundary layer flow, Can. J. Chem. Eng. 92 (1) (2014) 189–195.
[9] K. Luo, A.Y. Wei, Z.L. Wang, J.R. Fan, Fully-resolved DNS study of rotation behaviors of one and two particles settling near a vertical wall, Powder Technol. 245 (2013) 115–125.
[10] T. Samruamphianskun, P. Piumsomboon, B. Chalermsinsuwan, Computation of system turbulences and dispersion coefficients in circulating fluidized bed downer using CFD simulation, Chem. Eng. Res. Des. 90 (12) (2012) 2164–2178.
[11] R. Li, M. Pellegrini, H. Ninokata, M. Mori, A numerical study on turbulence attenuation model for liquid droplet impingement erosion, Ann. Nucl. Energy 38 (6) (2011) 1279–1287.
[12] B.K. Sapra, Y.S. Mayya, A. Khan, F. Sunny, S. Ganju, H.S. Kushwaha, Aerosol studies in a nuclear aerosol test facility under different turbulence conditions, Nucl. Technol. 163 (2) (2008) 228–244.
[13] M.P. Kissane, F. Zhang, M.W. Reeks, Dust in HTRs: its nature and improving prediction of its resuspension, Nucl. Eng. Des. 251 (2012) 301–305.
[14] T. Lind, Y. Ammar, A. Dehbi, S. Guntay, De-agglomeration mechanisms of TiO_2 aerosol agglomerates in PWR steam generator tube rupture conditions, Nucl. Eng. Des. 240 (8) (2010) 2046–2053.
[15] W.W. Grabowski, L.P. Wang, Growth of cloud droplets in a turbulent environment, Annu. Rev. Fluid Mech. 45 (2013) 293–324.
[16] A. Pumir, M. Wilkinson, Collisional aggregation due to turbulence, Annu. Rev. Condens. Matter Phys. 7 (2016) 141–170.
[17] M.R. Maxey, The gravitational settling of aerosol-particles in homogeneous turbulence and random flow-fields, J. Fluid Mech. 174 (1987) 441–465.
[18] S. Sundaram, L.R. Collins, Collision statistics in an isotropic particle-laden turbulent suspension. 1. Direct numerical simulations, J. Fluid Mech. 335 (1997) 75–109.
[19] L.P. Wang, A.S. Wexler, Y. Zhou, Statistical mechanical description and modelling of turbulent collision of inertial particles, J. Fluid Mech. 415 (2000) 117–153.
[20] G.D. Jin, G.W. He, L.P. Wang, Large-eddy simulation of turbulent collision of heavy particles in isotropic turbulence, Phys. Fluids 22 (5) (2010) 055106.
[21] K. Gustavsson, B. Mehlig, Ergodic and non-ergodic clustering of inertial particles, Europhys. Lett. 96 (6) (2011) 60012.
[22] J. Bec, Multifractal concentrations of inertial particles in smooth random flows, J. Fluid Mech. 528 (2005) 255–277.
[23] J. Bec, M. Cencini, R. Hillerbrand, Heavy particles in incompressible flows: the large Stokes number asymptotics, Physica D-Nonlinear Phenomena 226 (1) (2007) 11–22.
[24] E.J.P. Woittiez, H.J.J. Jonker, L.M. Portela, On the combined effects of turbulence and gravity on droplet collisions in clouds: a numerical study, J. Atmos. Sci. 66 (7) (2009) 1926–1943.
[25] J. Bec, H. Homann, S.S. Ray, Gravity-driven enhancement of heavy particle clustering in turbulent flow, Phys. Rev. Lett. 112 (18) (2014) 184501.
[26] K. Gustavsson, S. Vajedi, B. Mehlig, Clustering of particles falling in a turbulent flow, Phys. Rev. Lett. 112 (21) (2014) 214501.
[27] Y. Park, C. Lee, Gravity-driven clustering of inertial particles in turbulence, Phys. Rev. Lett. 89 (6) (2014) 061004.
[28] H. Parishani, O. Ayala, B. Rosa, L.P. Wang, W.W. Grabowski, Effects of gravity on the acceleration and pair statistics of inertial particles in homogeneous isotropic turbulence, Phys. Fluids 27 (3) (2015) 033304.
[29] P.J. Ireland, A.D. Bragg, L.R. Collins, The effect of Reynolds number on inertial particle dynamics in isotropic turbulence. Part 2. Simulations with gravitational effects, J. Fluid Mech. 796 (2016) 659–711.
[30] B. Rosa, H. Parishani, O. Ayala, W.W. Grabowski, L.P. Wang, Kinematic and dynamic collision statistics of cloud droplets from high-resolution simulations, New J. Phys. 15 (2013) 045032.
[31] Y. Zhou, A.S. Wexler, L.P. Wang, Modelling turbulent collision of bidisperse inertial particles, J. Fluid Mech. 433 (2001) 77–104.
[32] L.P. Wang, Y. Xue, O. Ayala, W.W. Grabowski, Effects of stochastic coalescence and air turbulence on the size distribution of cloud droplets, Atmos. Res. 82 (1-2) (2006) 416–432.
[33] H.D. Yao, G.W. He, A kinematic subgrid scale model for large-eddy simulation of turbulence-generated sound, J. Turbul. 10 (19) (2009) 1–14.
[34] L.X. Zhou, Two-fluid turbulence modeling of swirling gas-particle flows - a review, Powder Technol. 314 (0032-5910) (2017) 253–263.
[35] N. Almohammed, M. Breuer, Modeling and simulation of agglomeration in turbulent particle-laden flows: a comparison between energy-based and momentum-based agglomeration models, Powder Technol. 294 (2016) 373–402.
[36] H. Grosshans, M.V. Papalexandris, Large eddy simulation of triboelectric charging in pneumatic powder transport, Powder Technol. 301 (2016) 1008–1015.
[37] G.W. He, G.D. Jin, Y. Yang, Space-time correlations and dynamic coupling in turbulent flows, Annu. Rev. Fluid Mech. 49 (1) (2017) 51–71.
[38] M.J. Cernick, S.W. Tullis, M.F. Lightstone, Particle subgrid scale modelling in large-eddy simulations of particle-laden turbulence, J. Turbul. 16 (2) (2015) 101–135.
[39] G.D. Jin, G.W. He, A nonlinear model for the subgrid timescale experienced by heavy particles in large eddy simulation of isotropic turbulence with a stochastic differential equation, New J. Phys. 15 (2013) 035011.
[40] I.M. Mazzitelli, F. Toschi, A.S. Lanotte, An accurate and efficient Lagrangian sub-grid model, Phys. Fluids 26 (9) (2014) 095101.
[41] B. Ray, L.R. Collins, Investigation of sub-Kolmogorov inertial particle pair dynamics in turbulence using novel satellite particle simulations, J. Fluid Mech. 720 (2013) 192–211.
[42] B. Shotorban, F. Mashayek, Modeling subgrid-scale effects on particles by approximate deconvolution, Phys. Fluids 17 (8) (2005) 081701.
[43] J.G.M. Kuerten, Subgrid modeling in particle-laden channel flow, Phys. Fluids 18 (2) (2006) 025108.
[44] G.I. Park, J. Urzay, M. Bassenne, P. Moin, A dynamic subgrid-scale model based on differential filters for LES of particle-laden turbulent flows, Tech. Rep., Annu. Res. Briefs 2015, Cent. Turbul. Res. Stanford Univ.. 2015, pp. 17–26.
[45] S. Stolz, N.A. Adams, An approximate deconvolution procedure for large-eddy simulation, Phys. Fluids 11 (7) (1999) 1699–1701.
[46] S. Stolz, N.A. Adams, L. Kleiser, An approximate deconvolution model for large-eddy simulation with application to incompressible wall-bounded flows, Phys. Fluids 13 (4) (2001) 997–1015.
[47] B. Shotorban, F. Mashayek, A stochastic model for particle motion in large-eddy simulation, J. Turbul. 7 (18) (2006) 1–13.
[48] P. Fede, O. Simonin, P. Villedieu, K. Squires, Stochastic modelling of the turbulent subgrid fluid velocity along inertial particle trajectories, Proceedings of the Summer Program, Center for Turbulence Research. 2006, pp. 247–258.
[49] B. Ray, L.R. Collins, A subgrid model for clustering of high-inertia particles in large-eddy simulations of turbulence, J. Turbul. 15 (6) (2014) 366–385.
[50] V. Eswaran, S.B. Pope, An examination of forcing in direct numerical simulations of turbulence, Comput. Fluids 16 (3) (1988) 257–278.
[51] J.P. Chollet, M. Lesieur, Parameterization of small scales of 3-dimensional isotropic turbulence utilizing spectral closures, J. Atmos. Sci. 38 (12) (1981) 2747–2757.
[52] J.P. Chollet, Two-point Closure Used for a Sub-grid Scale Model in Large Eddy Simulations, Springer Berlin Heidelberg. 1985, 62–72.
[53] F. Bianco, S. Chibbaro, C. Marchioli, M.V. Salvetti, A. Soldati, Intrinsic filtering errors of Lagrangian particle tracking in LES flow fields, Phys. Fluids 24 (4) (2012) 045103.
[54] G.W. He, R. Rubinstein, L.P. Wang, Effects of subgrid-scale modeling on time correlations in large eddy simulation, Phys. Fluids 14 (7) (2002) 2186–2193.
[55] G.W. He, M. Wang, S.K. Lele, On the computation of space-time correlations by large-eddy simulation, Phys. Fluids 16 (11) (2004) 3859–3867.
[56] J.G.M. Kuerten, A.W. Vreman, Can turbophoresis be predicted by large-eddy simulation? Phys. Fluids 17 (1) (2005) 011701.
[57] M.R. Maxey, J.J. Riley, Equation of motion for a small rigid sphere in a nonuniform flow, Phys. Fluids 26 (4) (1983) 883–889.
[58] O. Ayala, H. Parishani, L. Chen, B. Rosa, L.P. Wang, DNS of hydrodynamically interacting droplets in turbulent clouds: parallel implementation and scalability analysis using 2D domain decomposition, Comput. Phys. Commun. 185 (12) (2014) 3269–3290.
[59] G.W. He, J.B. Zhang, Elliptic model for space-time correlations in turbulent shear flows, Phys. Rev. E 73 (5) (2006) 055303(R).
[60] G.W. He, G.D. Jin, X. Zhao, Scale-similarity model for Lagrangian velocity correlations in isotropic and stationary turbulence, Phys. Rev. E 80 (6) (2009) 066313.
[61] X. Zhao, G.W. He, Space-time correlations of fluctuating velocities in turbulent shear flows, Phys. Rev. E 79 (4) (2009) 046316.